Pergamon

Int. J. Heat Mass Transfer. Vol. 38, No. 16, pp. 2925–2934, 1995

0017–9310/95 $9.50+0.00

0017–9310(95)00085–2

Optimization of pulsating heaters in forced convection

A. M. MOREGA, J. V. C. VARGAS and A. BEJAN†

Department of Mechanical Engineering and Materials Science, Duke University, Durham, NC 27708-0300, U.S.A.

(*Received* 10 *December* 1994 *and in final form* 27 *February* 1995)

Abstract—This is a theoretical, numerical and experimental study that shows how to optimize the performance of on and off pulsating heaters in forced convection. Scale analysis shows that there exists an optimal heat pulse interval or frequency that maximizes the overall thermal conductance between the heater and the free stream U_∞. Numerical results for a flat plate heater and experimental results for a cylinder in cross-flow validate the theory. Numerically it is shown that the optimal pulsating regime can be identified accurately by using a complete simulation of the flow and temperature field around the heater. Boundary layer simplified numerical methods fail to simulate the short-times (high frequency) range of the process. The maximized overall conductance of a pulsating heater does not exceed the conductance associated with a steady (continuous) heater. The experimental and numerical results are nondimensionalized and correlated by using the scales recommended by theory. When the 'on' and 'off' intervals are comparable, the optimal heat pulse interval is approximately 0.1 L/U_∞, where L is the scale of the swept length of the heater shape. This conclusion also applies to a pulsating heater embedded in a porous medium with uniform flow.

1. INTRODUCTION

A new trend in heat transfer research is represented by the interest in pulsating heat transfer, in both forced and natural convection. The main theme of this activity is that the pulsation can be tuned to the natural time scale of the flow, such that the thermal contact between wall and flow is maximized. The flow configurations and potential applications are extremely diverse, as pulsations can be built into the fluid flow, the wall heating pattern, or both.

The current literature on time-dependent heat transfer with pulsating near-stagnation flows was reviewed by Mladin and Zumbrunnen [1]. The optimization of thermal contact in this configuration is important in the design of jet impingement techniques for cooling electronics [2]. Configurations in which the wall heating is pulsed were optimized, by Zumbrunnen [3] for stagnation flow, by Kazmierczak and Chinoda [4], Mantle *et al.* [5] and Lage and Bejan [6] for natural convection in an enclosed fluid, and by Antohe and Lage [7] for natural convection in an enclosed saturated porous medium. One conclusion of these studies is that each flow has a natural frequency that, if matched to the wall heating pulses, holds the key to maximizing the overall heat transfer between the wall and the fluid.

In this paper we pursue the same fundamental question in the much simpler and more basic configuration of external forced convection. We seek to determine the optimal heat pulse characteristics of heaters of several shapes immersed in free streams. The study begins with a theoretical argument that identifies the proper scales of the time-dependent phenomenon, and outlines the course of the optimization process. Next, we rely on complete numerical simulations to determine accurately the optimal pulsating heating regime for a flat-plate heater parallel to an external stream. In the experiments that conclude the paper, we show that heaters of other shapes (e.g. cylinder in cross-flow) can be optimized in the laboratory, and that the optimal pulsating heating regime is predicted adequately by the nondimensional results developed theoretically and numerically.

2. SCALE ANALYSIS

The existence of an optimal frequency for pulsating heating in forced convection can be anticipated based on order of magnitude analysis. Consider for this purpose the configuration of Fig. 1, where the plane wall of length L is parallel to a uniform free stream (U_∞, T_∞). The period of the pulsating heat transfer process is t_1+t_2. During the time interval of length t_1, the entire surface releases heat into the fluid, and its temperature rises above the free stream temperature.

Let T_0 be the order of magnitude of the surface temperature $T_w(x,t)$ during the heating interval (note that in scale analysis T_w does not have to be assumed uniform). Similarly, L is the scale of the swept length of the body, which in Fig. 1 is a flat plate, and a cylinder of swept length scale D in the experimental

†Author to whom correspondence should be addressed.

NOMENCLATURE

B_z bias limit of z
f Blasius function, equation (23)
f the group $Nu_D/Pe_D^{1/2}$, equation (25)
F double integral, equations (14), (15)
k thermal conductivity
L length scale, length of flat plate
$\overline{Nu}$ overall time-averaged Nusselt number for flat plate, equation (14)
Nu_D overall time-averaged Nusselt number for cylinder, equation (25)
p pressure
P_z precision limit of z
Pe Peclet number of flat plate, $U_\infty L/\alpha$
Pe_D Peclet number of cylinder, $U_\infty D/\alpha$
Pr Prandtl number, ν/α
q'' heat flux
$\bar{q}''$ average heat flux, equation (5)
Q'' heat interaction per unit area, equation (4)
Re Reynolds number for flat plate, $U_\infty L/\nu$
Re_D Reynolds number for cylinder, $U_\infty D/\nu$
t time
t_1 'on' interval
t_2 'off' interval
$\tilde{t}$ dimensionless time: tU_∞/L for flat plate, and tU_∞/D for cylinder
T temperature
T_{max} hot-spot temperature
T_0 surface temperature scale (Fig. 1), and surface temperature (Sections 3 and 4)
T_∞ free stream temperature
u, v velocity components
U_∞ free stream velocity
x, y coordinates, Fig. 1.

Greek symbols
α thermal diffusivity
η_B similarity variable, equation (23)
θ dimensionless temperature, equation (10)
ν kinematic viscosity
ξ, η dimensionless coordinates, equation (10).

Subscripts
$(\,)_{opt}$ optimal
$(\,)_*$ dimensionless variables, equation (19).

part of the paper (Section 5). During the next interval, t_2, the heat transfer is interrupted, and the wall is modeled as an adiabatic surface. During this second interval, the wall temperature $T_w(x, t)$ drops toward T_∞ because of the cooling effect provided by the free stream.

Let us assume that at the $t = 0$ start of the heating pulse t_1 the fluid layer that touches the wall is cold enough that its temperature is of the order of T_∞. The heat transfer from the T_0 wall to this fluid layer is mainly by unsteady conduction in the y direction, provided t does not exceed the time scale associated with one sweep of the wall, L/U_∞. In other words, the following scale analysis is restricted to time-dependent thermal diffusion in the near-wall region. This regime is present when

$$t \lesssim \frac{L}{U_\infty} \tag{1}$$

i.e. when the thermal boundary layer has not had time to develop, and the instantaneous wall heat flux scale is

$$q'' \sim \frac{k(T_0 - T_\infty)}{(\alpha t)^{1/2}}. \tag{2}$$

If the heating interval t_1 does not exceed the sweep time,

$$t_1 \lesssim \frac{L}{U_\infty} \tag{3}$$

the energy released per unit area during the t_1 interval can be estimated by integrating equation (2),

$$Q'' = \int_0^{t_1} q'' \, dt \sim k(T_0 - T_\infty)\left(\frac{t_1}{\alpha}\right)^{1/2}. \tag{4}$$

The heat transferred from the wall during the subsequent t_2 interval is zero. Of practical interest is the heat flux averaged over an entire cycle $t_1 + t_2$, namely

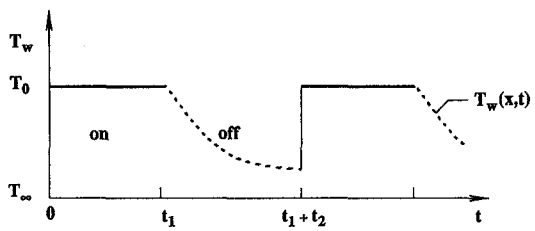

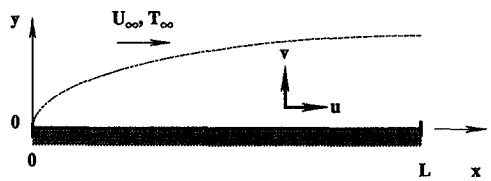

Fig. 1. Laminar boundary layer flow over a wall with pulsating heat release.

$$\bar{q}'' = \frac{Q''}{t_1+t_2} \sim \frac{k(T_0-T_\infty)}{\alpha^{1/2}} \cdot \frac{t_1^{1/2}}{t_1+t_2}. \quad (5)$$

The design of the heat pulse has two degrees of freedom, t_1 and t_2. The effect of the t_2 interval is such that $\bar{q}''$ increases monotonically as t_2 decreases, i.e. as the heating process approaches the continuous mode. This trend, however, is valid only if t_2 is greater than the sweep time,

$$t_2 \gtrsim \frac{L}{U_\infty}. \quad (6)$$

If t_2 is smaller than the sweep time, the assumption made above equation (1) is not valid because there will not be enough time for the wall region to be replenished by cold fluid.

A more interesting aspect of equation (5) is that $\bar{q}''$ has a maximum with respect to t_1. By solving $\partial\bar{q}''/\partial t_1 = 0$ we find that

$$t_{1,\text{opt}} \sim t_2. \quad (7)$$

This conclusion is not as general as it seems. In view of the opposing signs of the inequalities (3) and (6), the most we can say based on equation (7) is that when t_2 happens to be of the same order as the sweep time, the optimal heat pulse t_1 that maximizes $\bar{q}''$ is also of the same order as the sweep time, i.e.

$$t_{1,\text{opt}} \sim \frac{L}{U_\infty} \quad \text{when} \quad t_2 \sim \frac{L}{U_\infty}. \quad (8)$$

This demonstration of the existence of the t_1 optimum led us to the more practical problem of determining the exact relation between $\bar{q}''$ and t_1 and t_2. We investigated this problem numerically and experimentally, with the objective of identifying the pulsating heating design that maximizes the time-averaged thermal contact between the wall and the stream.

3. UNIFORM FLOW

The numerical work presented several challenges, especially with respect to the use of boundary layer theory in the construction of the numerical model. For this reason, we started with the simplifying assumption that the flow is uniform ($u = U_\infty, v = 0$), and constructed the numerical model and the optimization in the simplest possible setting. That preliminary work is reported in this section. In the following section (Section 4) we relaxed the uniform flow assumption and determined the effect of the Prandtl number on the optimization results.

The case where the stream sweeps the wall with uniform velocity corresponds to a fluid in the limit $Pr \to 0$ and to Darcy–Forchheimer flow in a porous medium saturated with fluid (e.g. ref. [8], pp. 52, 356). The energy equation for the time-dependent thermal boundary layer can be written nondimensionally as

$$\frac{\partial\theta}{\partial\tilde{t}} + \frac{\partial\theta}{\partial\xi} = \frac{\partial^2\theta}{\partial\eta^2} \quad (9)$$

where

$$\xi = \frac{x}{L} \quad \eta = \frac{y}{L}Pe^{1/2} \quad Pe = \frac{U_\infty L}{\alpha}$$

$$\tilde{t} = \frac{tU_\infty}{L} \quad \theta = \frac{T-T_\infty}{T_0-T_\infty}. \quad (10)$$

The initial and boundary conditions are

$$\begin{aligned} &\theta = 0 \quad \text{at} \quad \tilde{t} = 0 \\ &\theta = 1 \quad \text{at} \quad \eta = 0 \quad \text{and} \quad 0 < \tilde{t} \leqslant \tilde{t}_1 \\ &\frac{\partial\theta}{\partial\eta} = 0 \quad \text{at} \quad \eta = 0 \quad \text{and} \quad \tilde{t}_1 < \tilde{t} \leqslant \tilde{t}_1 + \tilde{t}_2 \\ &\theta \to 0 \quad \text{as} \quad \eta \to \infty \\ &\theta = 0 \quad \text{at} \quad \xi = 0 \end{aligned} \quad (11)$$

where we have assumed that during the heating interval the wall temperature is uniform and constant, $T_w = T_0$. The wall thermal boundary conditions were repeated during each subsequent cycle of duration $\tilde{t}_1 + \tilde{t}_2$. The evolution of the temperature field was simulated numerically until the initial transient died down and $\theta(\tilde{t}, \xi, \eta)$ became periodic.

The approach to the periodic state was determined based on the observed behavior of the heat flux averaged over the wall length L and a complete cycle $\tilde{t}_1 + \tilde{t}_2$. First, the instantaneous L-averaged heat flux was calculated from

$$q''(t) = \frac{1}{L}\int_0^L k\left(-\frac{\partial T}{\partial y}\right)_{y=0} \mathrm{d}x$$

$$= \frac{k}{L}(T_0-T_\infty)\left(\frac{U_\infty L}{\alpha}\right)^{1/2}\int_0^1 \left(-\frac{\partial\theta}{\partial\eta}\right)_{\eta=0} \mathrm{d}\xi. \quad (12)$$

The heat flux averaged over L and $\tilde{t}_1 + \tilde{t}_2$ was calculated next by using the left sides of equations (4) and (5):

$$\bar{q}'' = \frac{1}{\tilde{t}_1+\tilde{t}_2}\int_0^{t_1} q''(t)\,\mathrm{d}t. \quad (13)$$

The $\bar{q}''$ result was nondimensionalized as the overall time-averaged Nusselt number for the complete cycle,

$$\overline{Nu} = \frac{\bar{q}''L}{k(T_0-T_\infty)} = \left(\frac{U_\infty L}{\alpha}\right)^{1/2} F(\tilde{t}_1, \tilde{t}_2) \quad (14)$$

where F is the double integral

$$F(\tilde{t}_1, \tilde{t}_2) = \frac{1}{\tilde{t}_1+\tilde{t}_2}\int_0^{\tilde{t}_1}\left[\int_0^1 \left(-\frac{\partial\theta}{\partial\eta}\right)_{\eta=0} \mathrm{d}\xi\right]\mathrm{d}\tilde{t}. \quad (15)$$

The F function accounts for the effect of the heat pulse characteristics on the overall heat transfer between the wall and the stream. Note that F is the same as $\overline{Nu}/Pe^{1/2}$. We determined F numerically by first solving the transient thermal boundary layer problem (9)–(11) in the domain $0 < \xi < 1$ and

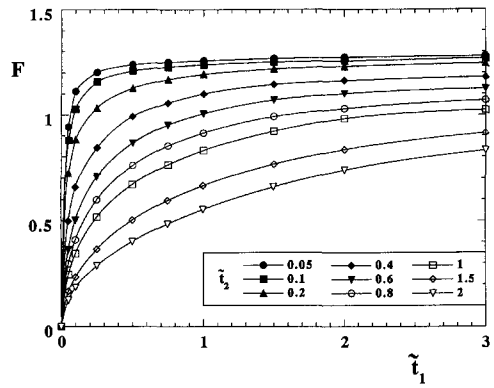

Fig. 2. The effect of the time intervals $\tilde{t}_1$ and $\tilde{t}_2$ on the overall time-averaged Nusselt number when the flow is uniform ($Pr \to 0$).

$0 < \eta < 5$. The finite-elements method consisted of using Galerkin weighted residuals, nine-node isoparametric quadratic elements, and the trapezoidal (implicit) algorithm with adaptive time step [9]. The local instantaneous heat flux on the wall became independent of grid size when the number of elements reached 1090, which is the number we retained for all the numerical runs. The resulting system of linear algebraic equations was solved for each time step through the quasi-Newton (one step) algorithm. The adaptive time integration scheme had the following restrictions: (i) a smallest time step in the range 10^{-5}–10^{-4}; (ii) a largest time step of 10^{-2}; and (iii) a local maximum relative time truncation error, d^n, of 10^{-3} at each time step, $\mathrm{d}\tilde{t}^{n+1} = \mathrm{d}\tilde{t}^n(10^{-3}/\|d^n\|)^{1/3}$, where $\mathrm{d}\tilde{t}^n$ and $\mathrm{d}\tilde{t}^{n+1}$ are the time increments at the steps n and $n+1$, and $\|\cdot\|$ is the Euclidian norm.

Six or seven consecutive cycles were required until the thermal boundary layer solution reached the periodic state. The results presented in Figs. 2 and 3 refer to the last cycle in each sequence. The calculation of the F function required special care, because during each $\tilde{t}_1$ interval (when the heating is 'on') the boundary temperature exhibited two types of behavior. At the start of the $\tilde{t}_1$ interval, the wall temperature was forced to a new and uniform value that differed markedly from the ξ-dependent distribution inherited from the end of the preceding $\tilde{t}_2$ interval. This initial shock was followed by a smooth variation in time for the wall temperature and heat flux. The smooth behavior continued into the $\tilde{t}_2$ interval, where the wall was adiabatic. To capture the true behavior of the wall heat flux during the entire cycle $\tilde{t}_1 + \tilde{t}_2$, it was necessary to avoid any numerical 'smoothing' of the solution, from one cycle to the next.

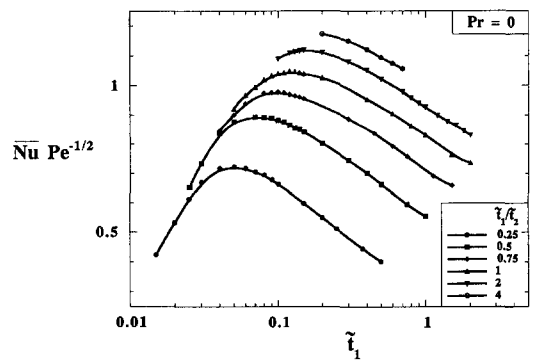

Fig. 3. Uniform flow : the maximization of the overall Nusselt number by selecting the pulse interval ($\tilde{t}_1$) when the pulse shape ($\tilde{t}_1/\tilde{t}_2$) is fixed.

The calculation of F started with the integral of equation (12),

$$\phi = \int_0^1 (-\partial\theta/\partial\eta)_{\eta=0}\,\mathrm{d}\xi,$$

which was available in tabular form at each time step of the last cycle. We fitted ϕ by least squares to an incomplete set of exponentials. After several trials and accuracy tests, we found that $\exp\{1, \tilde{t}^{-0.1}, \tilde{t}^{-0.2}, \tilde{t}^{-0.3}\}$ offered an excellent set, such that the relative error between the tabulated and curve-fitted ϕ values was less than 10^{-4}. Using these curve fits, we evaluated the time integrals

$$\int_0^{\tilde{t}_1} \phi\,\mathrm{d}\tilde{t}$$

analytically, and used them in the F definition (15).

We repeated this work for several combinations of $\tilde{t}_1$ and $\tilde{t}_2$, and obtained a two-dimensional table for $F(\tilde{t}_1, \tilde{t}_2)$. These data were fitted by least squares to incomplete sets of exponentials using the same method as in the preceding paragraph. For example, in Fig. 2 the curves drawn for F vs $\tilde{t}_1$ at constant $\tilde{t}_2$ show that F increases as $\tilde{t}_2$ decreases, in accordance with the scaling trend anticipated based on equation (5). It is worth noting that as the thermal boundary condition becomes continuous in time ($\tilde{t}_2 \to 0$), F approaches the exact solution for steady heat transfer from an isothermal wall bathed by uniform flow, $F = 1.128$ (e.g. ref. [8], pp. 52 and 358).

The data of Fig. 2 have been replotted in Fig. 3 as F vs $\tilde{t}_1$ when the ratio $\tilde{t}_1/\tilde{t}_2$ is held fixed. This presentation allows us to identify the optimal duration of the heating pulse, or the optimal period of the cycle, when the 'shape' of the pulse is fixed. The optimal $\tilde{t}_1$ values and the corresponding F maxima are listed in Table 1. The optimal duration of the heating pulse increases as the ratio $\tilde{t}_1/\tilde{t}_2$ increases.

It is interesting to note that the results of Fig. 3 agree in an order of magnitude sense with the optimum anticipated in equation (8). Figure 3 also shows that the F maximum falls under the ceiling value, $F = 1.128$, associated with steady heat transfer from an isothermal wall. The F maximum is quite sharp, and stresses the importance of identifying accurately the optimal period of the pulsating heating process.

4. NON-UNIFORM FLOW

The next question is how the conclusions of Fig. 3 change when the wall is swept by a common fluid such

Table 1. Numerical results for the optimal heating interval for maximum overall heat transfer (Sections 3 and 4.1)

	$Pr \to 0$		$Pr = 0.7$ $Re = 100$		$Pr = 7$ $Re = 100$	
$\tilde{t}_1/\tilde{t}_2$	$\tilde{t}_{1,\text{opt}}$	$\overline{Nu}_{\max} Pe^{-1/2}$	$\tilde{t}_{1,\text{opt}}$	$\overline{Nu}_{\max}$	$\tilde{t}_{1,\text{opt}}$	$\overline{Nu}_{\max}$
0.25	0.051	0.0761				
0.5	0.08	0.890	0.079	5.511	0.148	11.74
0.75	0.103	0.960				
1	0.126	1.042	0.081	6.266	0.161	14.26
∞ (steady)	—	1.128	—	7.63	—	17.68

as air or water ($Pr \gtrsim 0.5$). In such a case the flow is not uniform, and must be accounted for in the calculation of the time-dependent temperature and heat transfer. We pursued this question numerically by using two formulations: (i) a full Navier–Stokes formulation of the two-dimensional geometry of Fig. 1, and (ii) a boundary layer approximated model based on Blasius' solution for the flow field.

4.1. *Navier–Stokes model*

The nondimensional form of the fluid mechanics part of the problem is

$$\frac{\partial u_*}{\partial x_*} + \frac{\partial v_*}{\partial y_*} = 0 \tag{16}$$

$$u_* \frac{\partial u_*}{\partial x_*} + v_* \frac{\partial u_*}{\partial y_*} = -\frac{\partial p_*}{\partial x_*} + \frac{1}{Re}\left(\frac{\partial^2 u_*}{\partial x_*^2} + \frac{\partial^2 u_*}{\partial y_*^2}\right) \tag{17}$$

$$u_* \frac{\partial v_*}{\partial x_*} + v_* \frac{\partial v_*}{\partial y_*} = -\frac{\partial p_*}{\partial y_*} + \frac{1}{Re}\left(\frac{\partial^2 v_*}{\partial x_*^2} + \frac{\partial^2 v_*}{\partial y_*^2}\right) \tag{18}$$

where

$$(x_*, y_*) = \frac{(x, y)}{L} \quad (u_*, v_*) = \frac{(u, v)}{U_\infty}$$

$$p_* = \frac{p}{\rho U_\infty^2} \quad Re = \frac{U_\infty L}{\nu}. \tag{19}$$

The boundary conditions for the flow are

$$\begin{aligned} &u_* = 1\, v_* = 0 && \text{at} \quad x_* = 0 \\ &u_* = 0\, v_* = 0 && \text{at} \quad y_* = 0 \\ &\frac{\partial}{\partial x_*}(u_*, v_*) = 0 && \text{at} \quad x_* = 1 \\ &u_* = 1\, v_* = 0 && \text{as} \quad y_* \to \infty. \end{aligned} \tag{20}$$

The unsteady energy conservation equation that corresponds to this formulation is

$$\frac{\partial \theta}{\partial \tilde{t}} + u_* \frac{\partial \theta}{\partial x_*} + v_* \frac{\partial \theta}{\partial y_*} = \frac{1}{Pe}\left(\frac{\partial^2 \theta}{\partial x_*^2} + \frac{\partial^2 \theta}{\partial y_*^2}\right) \tag{21}$$

where θ, $\tilde{t}$ and Pe are defined in equation (10). The thermal wall conditions are the same as in equations (11).

The numerical method used to solve equations (16)–(21) was almost the same as in the preceding section. It was found that the $y_* \to \infty$ boundary, equation (20), can be replaced quite accurately with $y_* = 5$, such that the effect on the overall steady heat transfer rate ($\tilde{t}_2 \to 0$) is less than 1%. Since the problem is one of forced convection, the flow part was solved first, and the transient heat transfer part second. Special attention was paid to the approach to the quasisteady (periodic) regime. Figure 4 shows one of the tests used for this purpose. Each curve represents the average heat flux released by the wall at the first time step of each heating cycle (period). Two curves are drawn, one for $\theta = 1$ as initial condition (hot isothermal flow), and the other for $\theta = 0$ (cold isothermal flow). The figure shows that the periodic regime is reached after approximately 10 cycles.

The curve-fitting technique described in the preceding section was used again. This time the function basis was extended to $\exp\{1, \tilde{t}^{-0.1}, \tilde{t}^{-0.2}, \tilde{t}^{-0.3}, \tilde{t}^{-0.4}\}$. The F_* factor was defined simply as $F_* = \overline{Nu}$, instead of F of equation (14). The overall heat transfer results obtained for $Pr = 0.72$ and 7 at $Re = 100$ are summarized in Table 1 and Figs. 5 and 6. These also show the results obtained based on the boundary layer formulation, which is discussed later.

Figures 5 and 6 reinforce the conclusion that the overall heat transfer can be maximized with respect to the duration of the heat pulse ($\tilde{t}_1$) when the on/off ratio is fixed. As in the low Pr limit (Fig. 3), the optimal 'on' interval is of the order $\tilde{t}_{1,\text{opt}} \sim 0.1$. The maximum $\overline{Nu}$ value is consistently lower than the

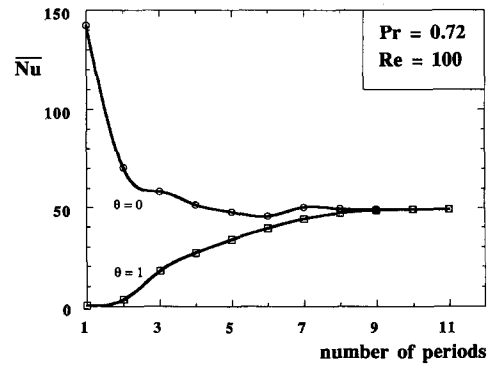

Fig. 4. Test for the approach to the periodic regime when $Pr = 0.72$, $Re = 100$, $\tilde{t}_1/\tilde{t}_2 = 1$ and $\tilde{t}_1 = 0.08$.

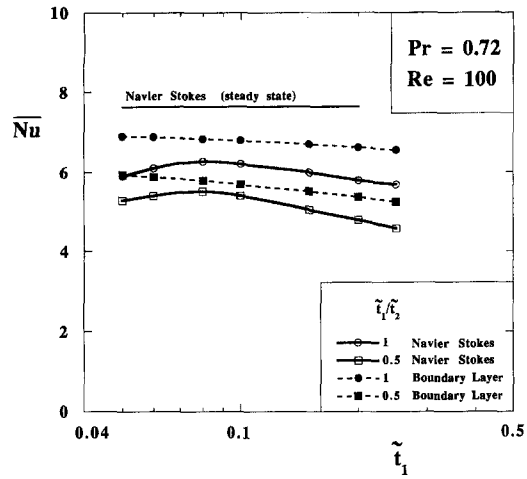

Fig. 5. Numerical results for averaged overall heat transfer when $Pr = 0.72$ and $Re = 100$.

value reached when the heating process is steady ($\tilde{t}_2 \to 0$), in agreement with the scaling prediction made in equation (5).

4.2. *Boundary layer model*

In this second two-dimensional formulation, we assumed that $u(x, y)$ and $v(x, y)$ are available from the classical Blasius solution (e.g. ref. [8], pp. 46–49). The nondimensional unsteady energy equation is

$$\frac{\partial\theta}{\partial\tilde{t}} + f'\frac{\partial\theta}{\partial\xi} + \left(\frac{Pr}{\xi}\right)^{1/2}(\eta_B f' - f)\frac{\partial\theta}{\partial\eta} = \frac{\partial^2\theta}{\partial\eta^2} \qquad (22)$$

where $\tilde{t}$, θ, ξ, and η are defined in equation (10), $f(\eta_B)$ is Blasius' function, and

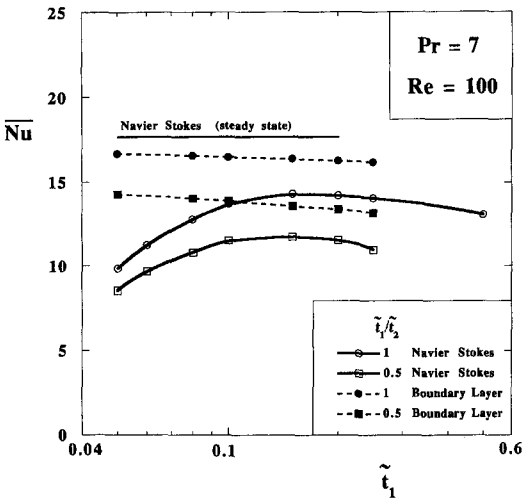

Fig. 6. Numerical results for averaged overall heat transfer when $Pr = 7$ and $Re = 100$.

$$\eta_B = \frac{\eta}{(\xi Pr)^{1/2}}, \quad u = U_\infty f'(\eta_B)$$

$$v = \frac{1}{2}\left(\frac{vU_\infty}{x}\right)^{1/2}(\eta_B f' - f). \qquad (23)$$

The boundary conditions are

$$\begin{aligned}
&\theta = 0 \quad \text{at} \quad \tilde{t} = 0\\
&\theta = 0 \quad \text{at} \quad \xi = 0\\
&\frac{\partial\theta}{\partial\xi} = 0 \quad \text{at} \quad \xi = 1\\
&\theta = 1 \quad \text{at} \quad \eta = 0 \quad \text{during } \tilde{t}_1\\
&\frac{\partial\theta}{\partial\eta} = 0 \quad \text{at} \quad \eta = 0 \quad \text{during } \tilde{t}_2\\
&\theta = 0 \quad \text{as} \quad \eta \to \infty \quad (\text{numerically}, \eta = 6). \qquad (24)
\end{aligned}$$

The F factor that was monitored was defined in Section 3, namely $F = \overline{Nu}\, Pe^{-1/2}$. The flow part of the problem (the Blasius problem) was solved using a Runge–Kutta 4th/5th order adaptive scheme with error control (10^{-6}) per η_B step. This tight control produced a sufficiently dense discrete set of (η_B, f, f') points that guaranteed a locally accurate interpolation scheme for determining the (η_B, f, f') values needed to substitute in equation (22). The energy equation was solved using a homemade code based on the ADI algorithm introduced by Douglass and Gunn, as presented by Peyret and Taylor [10]. The grid was uniform. The second-order accuracy of the scheme was preserved by making suitable approximations in the geometrical splitting of equation (22). The scheme is unconditionally stable because the coefficients of the convective terms are independent of the unknown θ. However, to avoid the 'pollution' caused by the boundary conditions and the anisotropy of the model, a suitable determined largest time step was used [10]. Space limitations force us to skip over several non-trivial aspects of the work done to ensure the accuracy of the results.

Figures 5 and 6 show the results obtained with the boundary layer model, next to the results based on the full Navier–Stokes model. The main conclusion is that the boundary layer formulation does not capture the physics of the heat transfer phenomenon at short 'on' intervals, and the calculated $\overline{Nu}$ does not reveal a maximum vs $\tilde{t}_1$. The reason is that at short times the temperature field has not had enough time to develop into a thermal (convective) boundary layer. This conclusion is supported by a companion study of the maximization of natural convection heat transfer from a wall with pulsating heating [11]. It is an important conclusion, because it makes necessary the numerical modeling based on the full Navier–Stokes equations (Section 4.1). The boundary layer method is, as expected, more expedient and captures at least approximately the effect of changing the on/off time ratio $\tilde{t}_1/\tilde{t}_2$.

5. EXPERIMENTS

We conducted a series of forced convection experiments in air to demonstrate the *existence* of an optimal heat pulse interval for maximum overall thermal conductance between the heater surface and the air stream. The experiments were performed using a single cylinder in cross-flow, with pulsed heat generation rate in the cylinder. This configuration was selected in order to test the scale analysis of Section 2, which is supposed to be valid for heaters of any shape immersed in a free stream. The ultimate objective of these experiments was to demonstrate that the optimization executed numerically for plate heaters (Section 4) can be performed experimentally for heaters of other shapes.

5.1. *Experimental apparatus*

Figure 7 shows the main components of the experimental facility. A heat generating cylinder was held horizontally in a wind tunnel connected to a suction fan. The internal dimensions of the wind tunnel are $11 \times 13 \times 60$ cm. The electric heater (CHROMALOX model 3618K532, maximum power 450 W at 120 V) was inserted with a tight fit inside a brass tube with an outer diameter of 1.27 cm. Three precision thermistors type YSI44004 were embedded in the outer surface of the brass tube. A layer of heat sink silicone was placed between thermistors and brass. High conductivity epoxy was used to attach the thermistors to the tube surface. Two thermistors were positioned at the extremities of the tube, and a third was installed in the middle. Convection is the dominant mechanism (or thermal resistance) because the brass cylinder has high thermal conductivity, and the device is bathed by a stream of air.

The function of the thermistors was to measure the instantaneous temperature distribution on the cylinder surface, and to identify the hot spot temperature (T_{max}) during the on and off cycle. A fourth thermistor monitored the free stream temperature during each run. The readings were taken with an ohmmeter capable of measuring resistances as small as $10^{-2}\Omega$. In this way we were able to evaluate through direct measurements of temperature, time and air velocity, the group

$$f = \frac{Nu_D}{Pe_D^{1/2}} = \frac{q''D}{(1+t_2/t_1)k(T_{max}-T_\infty)}\left(\frac{\alpha}{U_\infty D}\right)^{1/2} \quad (25)$$

where $Pe_D = U_\infty D/\alpha$. In the Nu_D definition, q'' is the uniform heat flux released by the cylinder surface during the t_1 interval, and $q''/(1+t_2/t_1)$ is the heat flux averaged over a complete cycle. The function f of equation (25) should not be confused with the Blasius function of equation (23).

We designed and built the adjustable electronics needed to make our own square pulse heat generator. The intervals of the on and off cycle are controlled by a dual timer integrated circuit, which controls a relay that interrupts the heater power supply. The time ratio can be adjusted. In the experiments we used $t_1/t_2 = 1$ and 0.5. All the time settings were adjusted using a chronometer with a bias limit of ± 0.01 s. The power input to the electric heater was held constant during each 'on' interval of each run. One power setting for the heater was used, 0.115 W.

We found that we had to use a low Reynolds number $Re_D = U_\infty D/\nu$ to ensure that the measured time intervals remained at least one order of magnitude higher than the time bias limit. We did this by regulating the fan speed through a variable resistor, and measuring the air velocity with an anemometer with a bias limit of $\pm 3\%$. In this way we fixed the air speed at $Re_D = 4$ in all the runs: we used only one power setting for the fan, which means that the free stream velocity was the same in all the runs, accounting of course for the uncertainty in the measurements, which we did. Since at low velocities the accuracy of the anemometer is not guaranteed by the manufacturer, we double checked the measured $Re_D = 4$ value in a special run with steady-state heat flux ($t_2 = 0$). The Nu_D value determined experimentally based on equation (25) was $Nu_D = 1.43$, while the value recommended for $Re_D = 4$ and $Pr = 0.72$ by a correlation based on data from many independent sources [12] is $Nu_D = 1.28$. These findings are consistent with the known fact that the correlations of ref. [12] can predict Nu_D values that are up to 20% smaller than those furnished by experiments [13].

5.2. *Procedure*

The thermistor bias limits were determined by calibration for one thermistor at a time. The thermistor was immersed in a constant temperature bath, and a total of 64 temperature measurements were made at 20, 30, ..., 80°C. The largest standard deviation of these measurements was 0.0006°C, therefore the bias limit was set at ± 0.001°C for all the thermistors. This bias limit is in agreement with the ± 0.0003°C bias limit of the same thermistors in a natural convection experiment [14], and with the ± 0.0005°C bias limit listed in an instrumentation handbook [15]. As we mentioned already, we performed our own calibration to confirm this information.

The precision and bias limits in the measurement of the group $f = Nu_D/Pe_D^{1/2}$ and $\tilde{t}_1$ were calculated using the propagation line of Kline and McClintock [16],

$$\frac{P_f}{f} = \frac{P_{\Delta T}}{\Delta T} \quad (26)$$

$$\frac{B_f}{f} = \left\{\frac{[1+(t_2/t_1)^2]}{(1+t_2/t_1)^2}\cdot\left(\frac{B_{t_1}}{\tilde{t}_1}\right)^2 + \left(\frac{B_{U_\infty}}{2U_\infty}\right)^2\right\}^{1/2} \quad (27)$$

$$\frac{B_{\tilde{t}_1}}{\tilde{t}_1} = \left[\left(\frac{B_{t_1}}{t_1}\right)^2 + \left(\frac{B_{U_\infty}}{U_\infty}\right)^2\right]^{1/2} \quad (28)$$

where $\Delta T = T_{max} - T_\infty$. We measured T_{max} and T_∞. The laboratory is a temperature controlled environment without windows, therefore the variations in

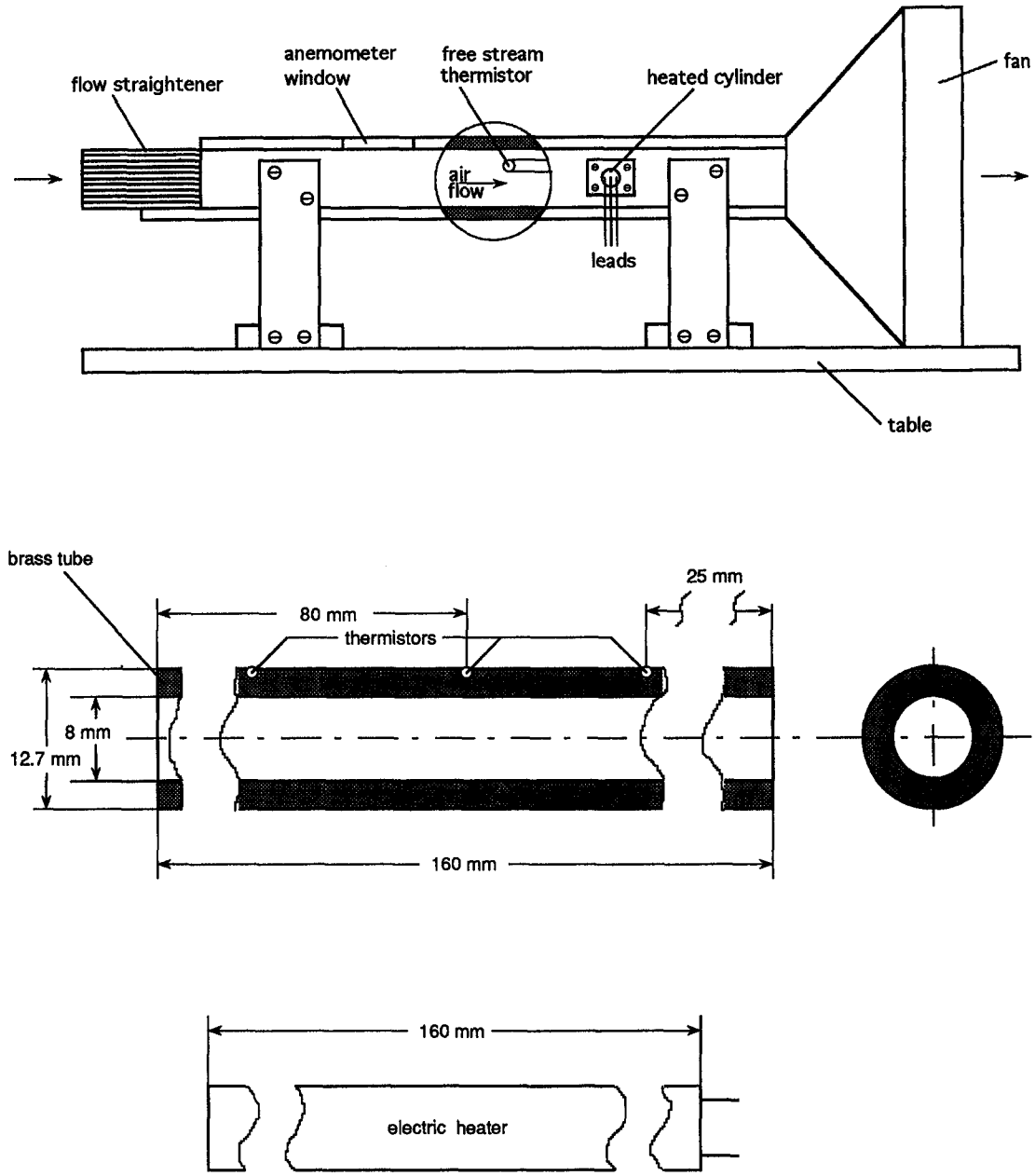

Fig. 7. The main features of the experimental apparatus : wind tunnel (top) and instrumented cylinder (bottom).

room pressure, temperature and humidity were negligible. In the calculation of the precision limit for the measured group f, the contributions made by the precision limits of t_1, t_2, D, q'', U_∞ and the tabulated physical properties were found to be negligible relative to the precision limit of ΔT. The time contributions are negligible because once the electronic timer is adjusted, the time intervals are reproduced identically in all the runs. The same observation applies to the air velocity: once the fan speed is calibrated through an appropriate power setting, U_∞ is reproduced identically in subsequent runs. In the calculation of the bias limit for f, the time bias limit and the anemometer bias limit are the most important contributions, because the temperature bias limit provided by the thermistors is very small in comparison with the bias limit of the anemometer and the time bias limit of the chronometer used in the timer adjustment. The precision limit for the measured $\tilde{t}_1$ is negligible relative to the bias limit in the calculation of the uncertainty, because an electronic time control method was used. Worth noting is that in the case of a cylinder the dimensionless times are based on D,

$$(\tilde{t}_1, \tilde{t}_2) = \frac{U_\infty}{D}(t_1, t_2). \tag{29}$$

Table 2. Relative uncertainties in the experiments with a cylinder in cross-flow ($Re_D = 4$, $D = 1.27$ cm)

$\tilde{t}_1/\tilde{t}_2 = 0.5$				$\tilde{t}_1/\tilde{t}_2 = 1$			
$\tilde{t}_1$	$U_{\tilde{t}_1}/\tilde{t}_1$	f	U_f/f	$\tilde{t}_1$	$U_{\tilde{t}_1}/\tilde{t}_1$	f	U_f/f
0.05	0.085	0.568	0.062	0.05	0.085	0.676	0.059
0.08	0.058	0.572	0.040	0.08	0.058	0.693	0.039
0.12	0.045	0.585	0.029	0.12	0.045	0.711	0.030
0.16	0.039	0.571	0.024	0.16	0.039	0.733	0.031
0.72	0.031	0.520	0.031	0.72	0.031	0.651	0.019

The precision limit for the temperature measurements was calculated as twice the standard deviation of each set (10 values per point) of observations for ΔT. The uncertainty limits for f and $\tilde{t}_1$ were calculated with the following formulas, and the results are summarized in Table 2,

$$\frac{U_f}{f} = \left[\left(\frac{P_f}{f}\right)^2 + \left(\frac{B_f}{f}\right)^2\right]^{1/2} \quad \frac{U_{\tilde{t}_1}}{\tilde{t}_1} = \frac{B_{\tilde{t}_1}}{\tilde{t}_1}. \tag{30}$$

5.3. *Results*

Figure 8 shows the measured effect of the pulse interval $\tilde{t}_1$ on the overall thermal conductance between the cylinder and the air stream. Ten runs at the same power setting are responsible for each of the points plotted in the figure. The results show that there is an optimal $\tilde{t}_1$ for maximum thermal conductance. Expressed in dimensionless terms, the optimal time is of order of 0.1, as in Figs. 3 and 5 for the plate heater.

We added to Fig. 8 the numerical results calculated in Section 4.1 for the plate heater. This superposition is appropriate in an order of magnitude sense, because in laminar forced convection on a flat plate in air $\overline{Nu}$ scales as $Pe^{1/2}$ or $Re^{1/2}$. The agreement between the numerical and experimental results is remarkable for two very important reasons: (1) the experiments involved a cylinder in cross-flow while the numerical simulations referred to a flat plate; and (2) the cylinder was a heater with uniform flux, while the flat plate had uniform temperature. In summary, Fig. 8 provides support for the scale analysis that preceded the numerical and experimental work.

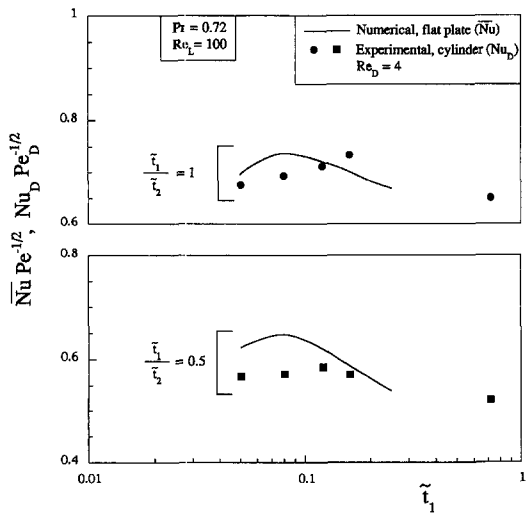

Fig. 8. Experimental results for the optimization of a cylindrical heater in cross-flow, and comparison with the numerical results for the plate heater.

6. CONCLUSION

We have presented a theoretical, numerical and experimental study in which we considered the optimization of the heat transfer performance of pulsating heaters in forced convection. The empirical results validate the scale analysis, which predicted a certain heat pulse interval such that the heater–fluid thermal conductance is maximum.

We showed that in simple geometries, such as the flat plate parallel to a free stream (fluid, or saturated porous medium), the optimal regime of pulsating heat transfer can be determined accurately by relying on a complete numerical simulation of the flow and time-dependent temperature field (Section 4.1). We also found that boundary layer simplifications fail to capture the short-times (high frequency) range of the phenomenon.

In most other cases, the optimal pulsating heating regime can be determined experimentally. We illustrated the procedure by using a single cylindrical heater in cross-flow. It is important that when the results are nondimensionalized based on the proper scales of the time-dependent phenomenon, the optimization of the cylinder fits on the same nondimensional plot as that of the flat plate.

These conclusions stress the generality of the pulsating heating optimization process. They also stress the applicability of the present methods to the optimization of heaters with other shapes and surface thermal conditions. The optimization of pulsating heaters in natural convection is described in ref. [11].

Acknowledgement—This work was supported by the National Science Foundation and Conselho Nacional de Desenvolvimento Cientifico e Technologico—CNPq (Brazil). The numerical work was supported by a grant received from the North Carolina Supercomputing Center.

REFERENCES

1. E. C. Mladin and D. A. Zumbrunnen, Dependence of heat transfer to a pulsating stagnation flow on pulse characteristics, *J. Thermophys. Heat Transfer* **9,** 181–190 (1995).
2. G. P. Peterson and A. Ortega, Thermal control of electronic equipment and devices, *Adv. Heat Transfer* **20,** 181–314 (1990).
3. D. A. Zumbrunnen, Transient convective heat transfer in planar stagnation flows with time-varying surface heat flux and temperature, *J. Heat Transfer* **114,** 85–92 (1992).
4. M. Kazmierczak and Z. Chinoda, Buyoancy-driven flow in an enclosure with time periodic boundary conditions, *Int. J. Heat Mass Transfer* **35,** 1507–1518 (1992).
5. J. Mantle, M. Kazmierczak and B. Hiawy, The effect of temperature modulation on natural convection in a horizontal layer heated from below: high-Rayleigh-number experiments, *J. Heat Transfer* **116,** 614–620 (1994).
6. J. L. Lage and A. Bejan, The resonance of natural convection in an enclosure heated periodically from the side, *Int. J. Heat Mass Transfer* **36,** 2027–2038 (1993).
7. B. V. Antohe and J. L. Lage, A dynamic thermal insulator: inducing resonance within a fluid saturated porous medium enclosure heated periodically from the side, *Int. J. Heat Mass Transfer* **37,** 771–782 (1994).
8. A. Bejan, *Convection Heat Transfer*. Wiley, New York (1984).
9. FIDAP, *Theoretical Manual and Examples Manual*. Fluid Dynamics International, Evanston, IL, Revision 7.0 (1994).
10. R. Peyret and T. Taylor, *Computational Methods for Fluid Flow*. Springer, New York (1990).
11. J. V. C. Vargas and A. Bejan, Optimization principle for natural convection pulsating heating, *J. Heat Transfer* **118,** in press.
12. S. W. Churchill and M. Bernstein, A correlating equation for forced convection from gases and liquids to a circular cylinder in crossflow, *J. Heat Transfer* **99,** 300–306 (1977).
13. A. Bejan, *Heat Transfer*, p. 264. Wiley, New York (1993).
14. L. Howle, J. Georgiadis and R. Behringer, Shadowgraphic visualization of natural convection in rectangular-grid porous layers, *ASME HTD* **206-1,** 17–24 (1992).
15. J. W. Dally, W. F. Riley and K. G. McConnell, *Instrumentation for Engineering Measurements* (2nd Edn), p. 425. Wiley, New York (1993).
16. Editorial, *J. Heat Transfer* **115,** 6 (1993).